Cretaceous fossil reveals a new pattern in mammalian middle ear evolution

https://doi.org/10.1038/s41586-019-1792-0

Received: 23 April 2019

Accepted: 23 October 2019

Published online: 27 November 2019

Haibing Wang[1,2], Jin Meng[3] & Yuanqing Wang[1,2,4]*

The evolution of the mammalian middle ear is thought to provide an example of 'recapitulation'—the theory that the present embryological development of a species reflects its evolutionary history. Accumulating data from both developmental biology and palaeontology have suggested that the transformation of post-dentary jaw elements into cranial ear bones occurred several times in mammals[1,2]. In addition, well-preserved fossils have revealed transitional stages in the evolution of the mammalian middle ear[1,3,4]. But questions remain concerning middle-ear evolution, such as how and why the post-dentary unit became completely detached from the dentary bone in different clades of mammaliaforms. Here we report a definitive mammalian middle ear preserved in an eobaatarid multituberculate mammal, with complete post-dentary elements that are well-preserved and detached from the dentary bones. The specimen reveals the transformation of the surangular jaw bone from an independent element into part of the malleus of the middle ear, and the presence of a restricted contact between the columelliform stapes and the flat incus. We propose that the malleus–incus joint is dichotomic in mammaliaforms, with the two bones connecting in either an abutting or an interlocking arrangement, reflecting the evolutionary divergence of the dentary–squamosal joint[4]. In our phylogenetic analysis, acquisition of the definitive mammalian middle ear in allotherians such as this specimen was independent of that in monotremes and therians. Our findings suggest that the co-evolution of the primary and secondary jaw joints in allotherians was an evolutionary adaptation allowing feeding with unique palinal (longitudinal and backwards) chewing. Thus, the evolution of the allotherian auditory apparatus was probably triggered by the functional requirements of the feeding apparatus.

Mammalia Linnaeus, 1758
Multituberculata Cope, 1884
Eobaataridae Kielan-Jaworowska, Dashzeveg and Trofimov, 1987
Jeholbaatar kielanae gen. et sp. nov.

Etymology. *Jehol* derives from the Jehol Biota ecosystem of Cretaceous northeastern China; *baatar* (Mongolian), meaning hero, is a common suffix for Asian Cretaceous multituberculate names; *kielanae* honours the Polish palaeontologist Zofia Kielan-Jaworowska for her contribution to the study of multituberculates.

Holotype. A nearly complete skeleton (IVPP V20778; Fig. 1), housed in the Institute of Vertebrate Paleontology and Paleoanthropology, Beijing, China.

Locality and age. The specimen is from the Jiufotang Formation near Changzigou, Lingyuan City, Liaoning Province, China, dated to approximately 120 million years ago[5].

Diagnosis. Dental formula of $I^3{\cdot}C^0{\cdot}P^5{\cdot}M^2/I_1{\cdot}C_0{\cdot}P_3{\cdot}M_2$ (I, incisor; C, canine; P, premolar; M, molar; superscript and subscript denote upper and lower teeth, respectively), with the following multituberculate characteristics (Extended Data Figs. 1, 2): cranium dorsoventrally compressed; masseteric fossa anteriorly extending below lower premolars; lingual offset of M^2 relative to M^1; enlarged single lower incisor; blade-like P_4; definitive mammalian middle ear (Extended Data Figs. 3, 4). Among multituberculates, *Jeholbaatar* is referable to eobaatarids on the basis of: upper canines absent; I^3 transversely wide; and eight serrations and a posterolabial cusp on P_4. *Jeholbaatar* differs from most eobaatarids (except for *Eobaatar* and *Heishanbaatar*) in having eight serrations on P_4; differs from *Eobaatar* in having reduced P_{2-3}, more buccal cusps on M^1, and a ridged cusp row on P^5; differs from *Heishanbaatar* in having an oval lateral outline of P_3 and more cusps of lower molars; and differs from *Sinobaatar* in having a posterior cuspule on I^2, two cusp rows of P^5, and different cusp counts of upper and lower molars.

Phylogenetic analyses place *Jeholbaatar* within the monophyletic eobaatarids and closely related to *Sinobaatar* (Extended Data Figs. 5, 6). The body mass of *Jeholbaatar* is estimated to be approximately 50 g on the basis of its skull length[6] (see Supplementary Information).

[1]Key Laboratory of Vertebrate Evolution and Human Origins of Chinese Academy of Sciences, Institute of Vertebrate Paleontology and Paleoanthropology, Beijing, China. [2]Centre for Excellence in Life and Paleoenvironment, Chinese Academy of Sciences, Beijing, China. [3]Division of Paleontology, American Museum of Natural History, New York, NY, USA. [4]College of Earth and Planetary Sciences, University of Chinese Academy of Sciences, Beijing, China. *e-mail: wangyuanqing@ivpp.ac.cn

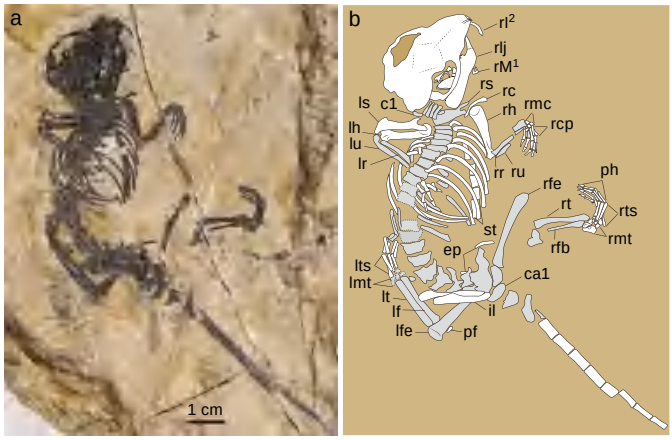

Fig. 1 | The Cretaceous multituberculate *Jeholbaatar kielanae*. a, Holotype (IVPP V20778) in dorsal view. **b**, Line drawing of the holotype. Grey shading indicates damaged elements. ca1, first caudal vertebra; c1, atlas; ep, epipubis; il, ilium; lf, left fibula; lfe, left femur; lh, left humerus; lmt, left metatarsals; lr, left radius; ls, left scapulocoracoid; lt, left tibia; lts, left tarsals; lu, left ulnar; pf, parafibula; ph, phalanges; rc, right clavicle; rcp, right carpals; rh, right humerus; rfb, right fibula; rfe, right femur; rI^2, right I^2; rl, right lower jaw; rmc, right metacarpals; rmt, right metatarsals; rM^1, right M^1; rr, right radius; rs, right scapulocoracoid; rt, right tibia; ru, right ulna; st, sternum.

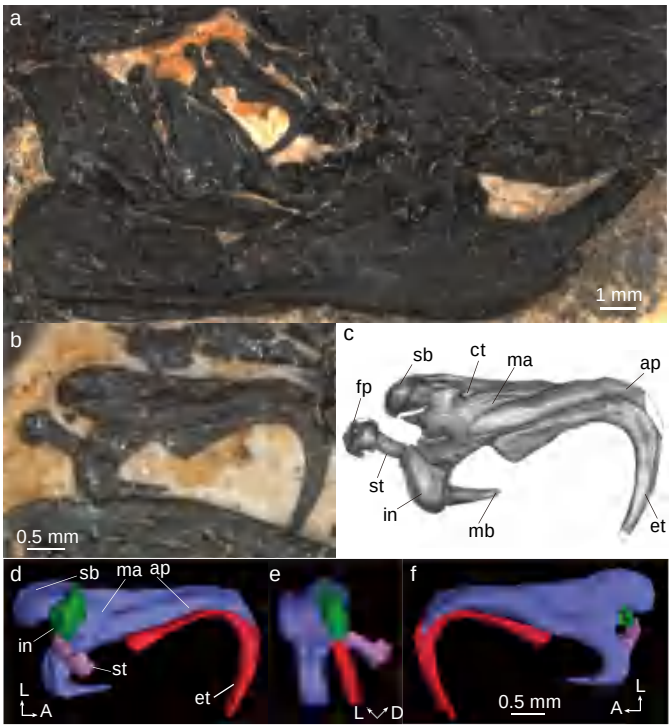

Fig. 2 | Middle-ear bones of *Jeholbaatar kielanae*. a, Left middle-ear bones, slightly displaced between the right lower jaw and braincase. **b**, Left middle ear bones exposed in dorsal view. **c**, Interpretative drawing of left ear bones. **d**–**f**, Reconstructions of left middle ear bones, showing articulation of these elements, in dorsal (**d**), posterior (**e**) and ventral (**f**) views; the surangular, the malleus body and the anterior process of the malleus are combined as a unit. A, anterior; ap, anterior process of malleus; ct, foramen for chorda tympani; D, dorsal; et, ectotympanic; fp, footplate of stapes; in, incus; L, lateral; ma, body of malleus; mb, manubrium of malleus; sb, surangular boss; st, stapes.

Jeholbaatar is inferred to be scansorial on the basis of its manual and pedal morphology, and the phalangeal index of its third digits is the greatest among multituberculates, with postcranials preserved (Fig. 1, Extended Data Fig. 7 and Extended Data Table 1). Given the morphology of the lower cheek teeth, we infer that *Jeholbaatar* is similar to *Eobaatar* in having an omnivorous diet, feeding on arthropods, worms and plant items[7]. The palinal jaw joint[4] and the distinct attachment for the masseter muscle suggest a unique palinal jaw movement while chewing (Extended Data Fig. 1).

The well-preserved left middle-ear bones are mediodorsally exposed and articulated nearly in anatomical position (Fig. 2 and Extended Data Figs. 3, 4). This unit is clearly detached from the dentary, as indicated by the absence of a sulcus on the lingual side of the dentary, as in other multituberculates; thus, *Jeholbaatar* has by definition the definitive mammalian middle ear (DMME)[8]. The stapes is columelliform–microperforate and distinct from the typical columelliform stapes of *Lambdopsalis*[9] in having a robust shaft, a less expanded stapedial footplate (the proximal end of the stapes), and a more basally positioned stapedial foramen (Extended Data Fig. 3). Laterally, the stapedial head—not exposed fully in dorsal view—is narrowed (relative to the proximal end) as in therian mammals, and articulates with the stapedial process (the long crus) of the incus through a restricted contact (relative to the broad end-on contact in other mammaliaforms[10]), preserving no sign of the extrastapes. The complete incus, previously unknown in a multituberculate, is slightly displaced ventrally, revealing its shape and orientation. The incus body is flat and lies medial to the transverse portion of the malleus body. Its morphology and small size suggest that the incus may not contact the squamosal dorsally. The proximal portion of the anterior process of the malleus is dorsally thicker than the transverse portion of the malleus body. A foramen, presumably for the chorda tympani, perforates the malleus (Extended Data Fig. 3). The malleus body bears a short manubrium projecting anteroventrally. The ventrolateral part of the malleus is thick and wedge-shaped, which we interpret as the remnant of the surangular. It consists of an anterior projection and a convex posterior end (surangular boss; Fig. 2). The posterior portion of the surangular extends posterolaterally and the posterodorsal surface of the surangular boss remains smooth and restricted medially by a distinct neck, which is reminiscent of an articular surface. The ectotympanic is large and roughly sickle-shaped with a gently posteriorly curved ventral limb and no anterior limb. The posterior portion of the horizontal limb is slightly expanded medially. The ectotympanic connects firmly to the malleus, suggesting that they may function as a unit.

The specimen provides important evidence regarding mammalian middle-ear evolution, revealing a unique configuration with more complete and complex components than those reported previously in Cretaceous multituberculates[11]. Under our phylogenetic framework, the DMME has evolved independently at least three times, in allotherians, monotremes and trechnotherians (Fig. 3).

Detachment of the auditory bones from the dentary was accompanied by loss of the anterior limb of the ectotympanic during development of the DMME, which evolved in parallel in monotremes, therians and allotherians (*Arboroharamiya* and *Jeholbaatar*)[4,12]. The hook-like ectotympanic is plesiomorphic for early mammals, as demonstrated by *Arboroharamiya* and *Jeholbaatar*, contrasting with the ring-like form of the Early Cretaceous *Ambolestes*[13].

The incus–stapes complex has been simplified in *Jeholbaatar* through a reduction in size and restricted incus–stapes contact. Whether the rod-like or the asymmetric bicrurate form represents the ancestral morphotype of the mammaliaform stapes is still disputed[14]. *Jeholbaatar* reveals a transitional stage in the evolution of the stapes, intermediate between the rod-like form (observed in cynodonts, *Arboroharamiya* and *Chaoyangodens*[4,10]) and the typical columelliform morphology (with a slender shaft, as seen in *Lambdopsalis*[9]). Although there are different interpretations of some previously reported multituberculate stapes[14], the robust shaft and less expanded footplate of the stapes in *Jeholbaatar* is distinct from the asymmetric bicrurate morphology (observed in *Pseudobolodon*[14]). This suggests several processes for

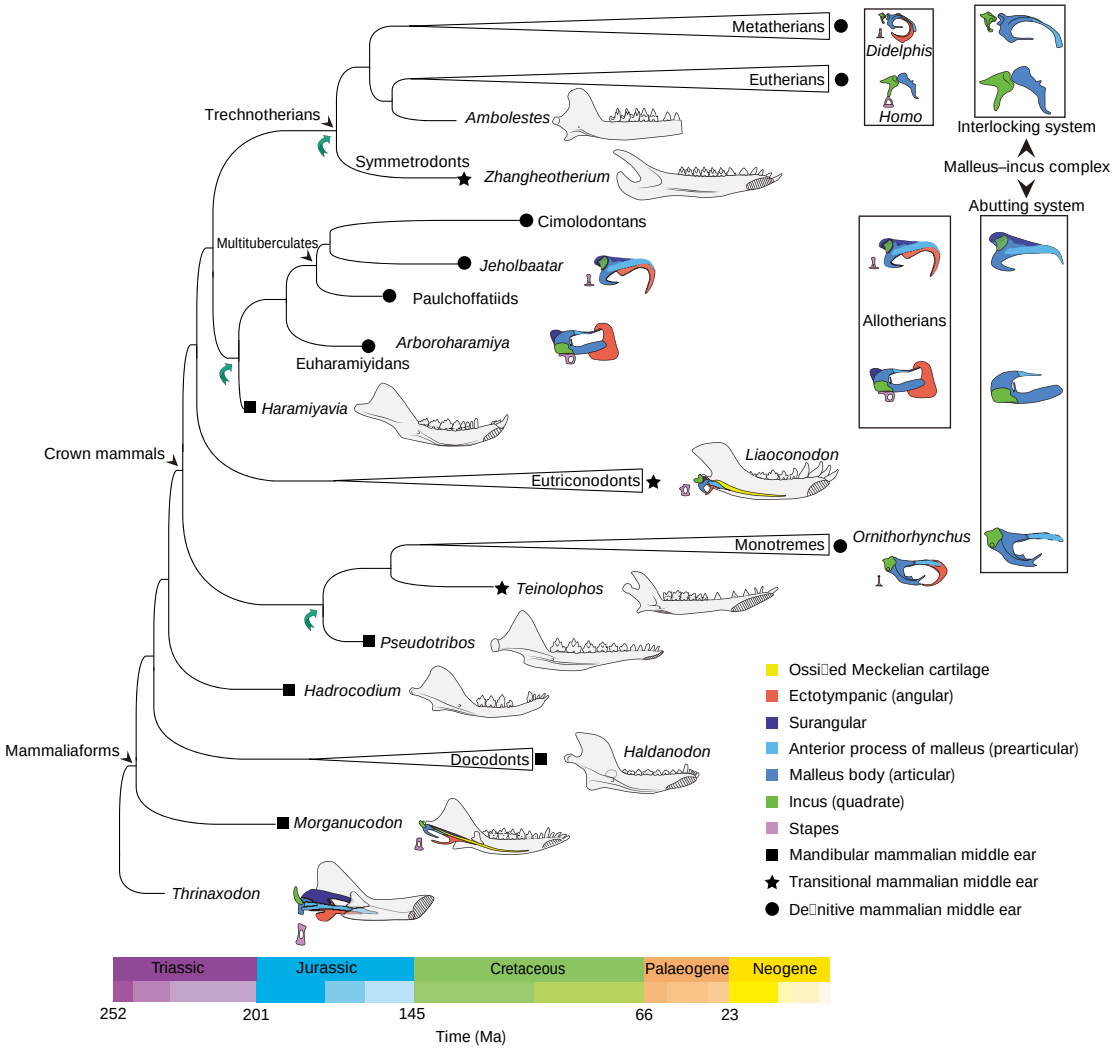

Fig. 3 | Evolution of the mammalian middle ear in different mammaliaform clades. This simplified phylogeny is based on the strict consensus of parsimony analysis (see Extended Data Fig. 5 and Supplementary Information). The green arrows denote independent evolution of the DMME in mammaliaforms. In the second column from the right are the middle-ear bone complexes of different taxa; at the right are the corresponding diagnostic configurations of the abutting and interlocking systems of the malleus–incus complex: in the abutting system, the malleus and incus contact dorsoventrally; in the interlocking system, this contact is rostrocaudal. Reconstructions of left middle ears are taken from the literature (see Methods and Supplementary Information). Graded colours in the key at the bottom denote Early, Middle and Late periods. Ma, million years ago.

evolution of the stapes in mammaliaforms, with independent acquisition of a bicrurate morphotype in *Pseudobolodon* and *Kryptobaatar*. The restricted incus–stapes contact of *Jeholbaatar* is derived by comparison with other mammaliaforms that have a broad end-on contact between these two bones. The development of the stapedial process of the incus, as an out-lever of the lever system during sound transition, is beneficial for the amplification of airborne sound[1].

Identification of the surangular in *Jeholbaatar* reinforces the argument that the remnant of the ancient 'reptilian' element exists in crown mammals (allotherians)[4]. It also fills a gap in the fossil record of the transformation of the surangular from an independent element to an accessory of the malleus[3,4], providing clues to the evolution of the surangular in mammaliaforms. In *Jeholbaatar*, the manubrium of the malleus is short and gradually tapers anterolaterally from the malleus body. This is the plesiomorphic condition, lacking the clear distinction between the manubrial base and the manubrium observed in other known Mesozoic mammaliaforms that have preserved the middle-ear bones (except *Arboroharamiya*)[3]. *Jeholbaatar* also provides evidence of a thickened malleus in a Mesozoic mammaliaform. This condition is defined specifically by the expression of the *Bapx1* gene in mice[15], implying similar embryonic development in *Jeholbaatar*.

The malleus–incus complex of *Jeholbaatar* is similar to that of *Arboroharamiya* and extant monotremes[4,12,16], with a dorsoventral contact of the malleus–incus complex. Given that the mammaliaform malleus–incus complex is derived from the primary joint in lower tetrapods, this raises an interesting issue concerning how the incus shifted dorsal to the malleus body during the transformation of the middle-ear bones. We propose that the articular configuration of the malleus–incus complex is dichotomic among mammaliaforms: the abutting system is characterized by a dorsoventral contact, as observed in monotremes, *Arboroharamiya*, and *Jeholbaatar*[4,16]; and the interlocking system has a rostrocaudal contact (and later hingle-like articulation), as observed in *Morganucodon*[17], *Liaoconodon* and other mammals except allotherians and monotremes[3]. This interpretation of the malleus–incus articulation contradicts previous proposals regarding other multituberculates[14,18]. However, in light of the unequivocal articulated middle-ear bones in *Jeholbaatar*, we postulate that the abutting system persisted in later multituberculate evolution. Whether this configuration is consistent in allotherians that have a mandibular mammalian middle ear (such as *Haramiyavia*) and transitional mammalian middle ear remains unknown. It has been proposed that the primary joint (malleus and incus) in mammals is determined by members of the *Gdf* gene family

(*Gdf5* and *Gdf6*)[15]. If all of these hypotheses are correct, then the developmental divergence of the primary joint (as reflected in the malleus–incus articulation) in mammaliaforms occurred deep in the Middle to Late Jurassic period, resulting in a shift in the position of the incus dorsal over the malleus (Extended Data Fig. 4). Despite the morphological distinction of the middle-ear bones between *Jeholbaatar* and *Arboroharamiya*, the configuration of the abutting system is coincident with the palinal jaw joint in multituberculates and euharamiyidans. The timing of the divergence of malleus–incus configurations (the abutting and interlocking systems) and the dichotomic morphotype of the squamosal–dentary jaw joint (palinal and hinge-like)[4] supports the hypothesis that the primary and secondary jaw joints co-evolved in allotherians.

The evolution of the DMME is associated with morphogenetic processes in the post-dentary bones, and causes of the detachment of Meckel's cartilage are hierarchical[1,19–21]. Palaeontological and developmental findings have rendered two conventional hypotheses for the degeneration of Meckel's cartilage (the brain-expansion hypothesis[22] and negative ontogenetic allometry of the middle-ear bones[23]) less plausible[20,24–26]. Instead, given the evidence from *Arboroharamiya* and *Jeholbaatar*, the evolution of the DMME in allotherians might be explained by biomechanical functional constraints during feeding[27,28], with co-evolution of the primary and secondary jaw joints being an adaptation for the unique palinal chewing of allotherians. Earlier acquisition of the DMME in allotherians also implies a shortened transitional mammalian middle-ear stage. The abutting-system configuration permitted longitudinal and vertical reduction of the middle-ear bones in some mammaliaforms. Detachment of the middle-ear bones (followed by better handling of biomechanical loads related to mastication on the medial side of the dentary[29]) and the abutting-system configuration could have increased the degree of food comminution per palinal power stroke in those allotherians with the DMME, and reduced the impact of feeding on the hearing apparatus. As such, selective pressure to detach the middle-ear bones (the hearing apparatus) in order to increase feeding efficiency could have been stronger in allotherians than in clades characterized by the interlocking system, showing that feeding was an important trigger in DMME evolution.

The homoplastic evolution of the DMME observed in fossils is consistent with developmental evidence, revealing diverse mechanisms for the detachment of Meckel's cartilage in different lineages[20]. The presence of the surangular remnant in *Jeholbaatar* might represent a recapitulation of the ancestral state, and suggests that evolution of the DMME could be an instance of von Baer's law of embryology[30]—although this hypothesis requires further investigation in a developmental context.

Online content

Any methods, additional references, Nature Research reporting summaries, source data, extended data, supplementary information, acknowledgements, peer review information; details of author contributions and competing interests; and statements of data and code availability are available at https://doi.org/10.1038/s41586-019-1792-0.

1. Luo, Z. X. Developmental patterns in Mesozoic evolution of mammal ears. *Annu. Rev. Ecol. Evol. Syst.* **42**, 355–380 (2011).
2. Maier, W. & Ruf, I. Evolution of the mammalian middle ear: a historical review. *J. Anat.* **228**, 270–283 (2016).
3. Meng, J., Wang, Y. & Li, C. Transitional mammalian middle ear from a new Cretaceous Jehol eutriconodont. *Nature* **472**, 181–185 (2011).
4. Han, G., Mao, F., Bi, S., Wang, Y. & Meng, J. A Jurassic gliding euharamiyidan mammal with an ear of five auditory bones. *Nature* **551**, 451–456 (2017).
5. He, H. Y. et al. Timing of the Jiufotang Formation (Jehol Group) in Liaoning, northeastern China, and its implications. *Geophys. Res. Lett.* **31**, L12605 (2004).
6. Millien, V. & Bovy, H. When teeth and bones disagree: body mass estimation of a giant extinct rodent. *J. Mamm.* **91**, 11–18 (2010).
7. Wilson, G. P. et al. Adaptive radiation of multituberculate mammals before the extinction of dinosaurs. *Nature* **483**, 457–460 (2012).
8. Allin, E. F. & Hopson, J. in *The Evolutionary Biology of Hearing* Ch. 28 (eds Webster, D. B. et al.) 587–614 (Springer, 1992).
9. Meng, J. The stapes of *Lambdopsalis bulla* (Multituberculata) and transformational analyses on some stapedial features in Mammaliaformes. *J. Vertebr. Paleontol.* **12**, 459–471 (1992).
10. Meng, J. & Hou, S. L. Earliest known mammalian stapes from an Early Cretaceous eutriconodontan mammal and implications for the evolution of mammalian middle ear. *Palaeontol. Pol.* **67**, 181–196 (2016).
11. Rougier, G. W., Wible, J. R. & Novacek, M. J. Middle-ear ossicles of the multituberculate Kryptobaatar from the Mongolian Late Cretaceous: implications for mammaliamorph relationships and the evolution of the auditory apparatus. *Am. Mus. Novit.* **3187**, 1–43 (1996).
12. Fleischer, G. Evolutionary principles of the mammalian middle ear. *Adv. Anat. Embryol. Cell Biol.* **55**, 3–70 (1978).
13. Bi, S. et al. An Early Cretaceous eutherian and the placental–marsupial dichotomy. *Nature* **558**, 390–395 (2018).
14. Schultz, J. A., Ruf, I. & Martin, T. Oldest known multituberculate stapes suggests an asymmetric bicrural pattern as ancestral for Multituberculata. *Proc. R. Soc. B* **285**, 20172779 (2018).
15. Tucker, A. S., Watson, R. P., Lettice, L. A., Yamada, G. & Hill, R. E. Bapx1 regulates patterning in the middle ear: altered regulatory role in the transition from the proximal jaw during vertebrate evolution. *Development* **131**, 1235–1245 (2004).
16. Zeller, U. in *Mammal Phylogeny: Mesozoic Differentiation, Multituberculates, Monotremes, Early Therians, and Marsupials* Ch. 8 (eds Szalay, F. S. et al.) 95–107 (Springer, 1993).
17. Kermack, K. A., Mussett, F. & Rigney, H. W. The skull of *Morganucodon*. *Zool. J. Linn. Soc.* **71**, 1–158 (1981).
18. Luo, Z. X. et al. New evidence for mammaliaform ear evolution and feeding adaptation in a Jurassic ecosystem. *Nature* **548**, 326–329 (2017).
19. Anthwal, N., Urban, D. J., Luo, Z.-X., Sears, K. E. & Tucker, A. S. Meckel's cartilage breakdown offers clues to mammalian middle ear evolution. *Nature Ecol. Evol.* **1**, 0093 (2017).
20. Urban, D. J. et al. A new developmental mechanism for the separation of the mammalian middle ear ossicles from the jaw. *Proc. R. Soc. B.* **284**, 20162416 (2017).
21. Lautenschlager, S., Gill, P. G., Luo, Z.-X., Fagan, M. J. & Rayfield, E. J. The role of miniaturization in the evolution of the mammalian jaw and middle ear. *Nature* **561**, 533–537 (2018).
22. Rowe, T. Coevolution of the mammalian middle ear and neocortex. *Science* **273**, 651–654 (1996).
23. Zeller, U. in *Morphogenesis of the Mammalian Skull* (eds Kuhn, H.-J. & Zeller, U.) 17–50 (Paul Parey, 1987).
24. Meng, J., Hu, Y. M., Wang, Y. Q. & Li, C. K. The ossified Meckel's cartilage and internal groove in Mesozoic mammaliaforms: implications to origin of the definitive mammalian middle ear. *Zool. J. Linn. Soc.* **138**, 431–448 (2003).
25. Wang, Y., Hu, Y., Meng, J. & Li, C. An ossified Meckel's cartilage in two Cretaceous mammals and origin of the mammalian middle ear. *Science* **294**, 357–361 (2001).
26. Ramírez-Chaves, H. E. et al. Mammalian development does not recapitulate suspected key transformations in the evolutionary detachment of the mammalian middle ear. *Proc. R. Soc. Lond. B* **283**, 20152606 (2016).
27. Crompton, A. W. & Parker, P. Evolution of the mammalian masticatory apparatus. *Am. Sci.* **66**, 192–201 (1978).
28. Allin, E. F. Evolution of the mammalian middle ear. *J. Morphol.* **147**, 403–437 (1975).
29. Crompton, A. W. & Hylander, W. L. in *The Ecology and Biology of Mammal-like Reptiles* (eds Hotton, N. et al.) 78–98 (Smithsonian Institute Press, 1986).
30. Abzhanov, A. von Baer's law for the ages: lost and found principles of developmental evolution. *Trends Genet.* **29**, 712–722 (2013).

Methods

Specimen preparation

At the early stage of preparation, the specimen was mainly exposed in dorsal view. After it was scanned using computed laminography, the skull was prepared from the backside of the slab to expose the skeletal morphology in ventral view.

Measurements

Skeletal elements were measured in ImageJ.

Figures

Middle ear reconstructions are based on the following references: *Thrinaxodon*, *Morganucodon* and *Didelphis*, ref. [28]; *Hadrocodium*, refs. [18,31]; *Pseudotribos*, ref. [32]; *Ornithorhynchus*, ref. [16]; *Teinolophos*, ref. [33]; *Liaoconodon*, ref. [3]; *Haramiyavia*, ref. [34]; *Arboroharamiya*, ref. [4]; *Zhangheotherium*, ref. [35]; *Ambolestes*, ref. [13]; *Haldanodon*, ref. [36].

Computed laminography

We carried out scanning using a microcomputed laminography system (developed by the Institute of High Energy Physics, Chinese Academy of Sciences (CAS) at the Key Laboratory of Vertebrate Evolution and Human Origins, CAS). The specimen was scanned with a beam energy of 60 kV and a flux of 40 μA at a resolution of 8.7 μm per pixel, using a 360° rotation with a step size of 1°. We reconstructed a total of 360 image slices with a size of 2,048 × 2,048 pixels using a modified Feldkamp algorithm developed by the Institute of High Energy Physics, CAS. Three-dimensional reconstruction of the auditory bones and teeth was conducted in VGStudio 3.0.

Taxonomic terminology

We use the node-based concept for crown clades of Mammalia; the term 'mammaliaforms' refers to taxa in Mammaliaformes[37]. Given recent studies[4,38], we regard Allotheria as a monophyletic group, and we test this hypothesis in our phylogenetic analyses. The content of the clade Euharamiyida follows previous work[4,38].

Phylogenetic analysis

We conducted two sets of phylogenetic analyses separately, using different data matrices to explore the placement of the new taxon in the mammaliaforms and multituberculates. The list of morphological characters for mammaliaform phylogeny follows ref. [4] (derived from refs. [38,39]), with separate analysis of two character matrices, A and B. We created a data matrix for multituberculate phylogeny analysis by adding new taxa and characters to expand the matrix in order to include 51 taxa and 130 characters on the basis of a newly published data matrix[40] (see Supplementary Information). Data matrices were edited in Mesquite v.3.03 and saved in NEXUS format for parsimony and Bayesian analysis. Bayesian analysis for mammaliaform or multituberculate phylogeny was run for 100 million Markov Chain Monte Carlo generations, with the first 25% discarded as 'burn-in', using the Mkv model for discrete morphological data and a gamma parameter for rate variation in MrBayes 3.2 (ref. [41]). Posterior probabilities were calculated to assess node robustness in MrBayes. Parsimony analysis was performed using TNT 1.5 with the New Technology Search method, implementing sectorial search, ratchet, drift and tree fusing, under equally weighted parsimony[42]. As is conventional for large datasets, 200 ratchet iterations, 100 drift cycles and 10 rounds of tree fusion were applied to conduct comprehensive searches during phylogenetic analysis. Two separate parsimony analyses were conducted, one with all characters unordered and the other with 19 characters ordered for the multituberculate data matrix, respectively. These ordered characters are 17, 25, 26, 29, 31, 32, 43, 46, 47, 48, 49, 51, 52, 55, 58, 59, 61, 72 and 85, as suggested previously[43,44]. Node support is given as Bremer support values in strict consensus of parsimony analysis, and as posterior probabilities (percentage) in 50% majority-rule consensus of Bayesian analysis.

Reporting summary

Further information on research design is available in the Nature Research Reporting Summary linked to this paper.

Data availability

The specimen (IVPP V20778) reported here is housed in the Institute of Vertebrate Paleontology and Paleoanthropology, Beijing, China. Character matrices are given in the Supplementary Information.

31. Luo, Z. X., Crompton, A. W. & Sun, A. L. A new mammaliaform from the early Jurassic and evolution of mammalian characteristics. *Science* **292**, 1535–1540 (2001).
32. Luo, Z. X., Ji, Q. & Yuan, C. X. Convergent dental adaptations in pseudo-tribosphenic and tribosphenic mammals. *Nature* **450**, 93–97 (2007).
33. Rich, T. H. et al. The mandible and dentition of the Early Cretaceous monotreme *Teinolophos trusleri*. *Alcheringa* **40**, 475–501 (2016).
34. Luo, Z. X., Gatesy, S. M., Jenkins, F. A. Jr, Amaral, W. W. & Shubin, N. H. Mandibular and dental characteristics of Late Triassic mammaliaform *Haramiyavia* and their ramifications for basal mammal evolution. *Proc. Natl Acad. Sci. USA* **112**, E7101–E7109 (2015).
35. Hu, Y., Wang, Y., Luo, Z. & Li, C. A new symmetrodont mammal from China and its implications for mammalian evolution. *Nature* **390**, 137–142 (1997).
36. Lillegraven, J. A. & Krusat, G. Cranio-mandibular anatomy of *Haldanodon exspectatus* (Docodonta; Mammalia) from the Late Jurassic of Portugal and its implications to the evolution of mammalian characters. *Rocky Mountain Geol.* **28**, 39–138 (1991).
37. Rowe, T. Definition, diagnosis and origin of Mammalia. *J. Vertebr. Paleontol.* **8**, 241–264 (1988).
38. Bi, S., Wang, Y., Guan, J., Sheng, X. & Meng, J. Three new Jurassic euharamiyidan species reinforce early divergence of mammals. *Nature* **514**, 579–584 (2014).
39. Krause, D. W. et al. First cranial remains of a gondwanatherian mammal reveal remarkable mosaicism. *Nature* **515**, 512–517 (2014).
40. Csiki-Sava, Z., Vremir, M., Meng, J., Brusatte, S. L. & Norell, M. A. Dome-headed, small-brained island mammal from the Late Cretaceous of Romania. *Proc. Natl. Acad. Sci. USA* **115**, 4857–4862 (2018).
41. Ronquist, F. et al. MrBayes 3.2: efficient Bayesian phylogenetic inference and model choice across a large model space. *Syst. Biol.* **61**, 539–542 (2012).
42. Goloboff, P. A., Farris, J. S. & Nixon, K. C. TNT, a free program for phylogenetic analysis. *Cladistics* **24**, 774–786 (2008).
43. Yuan, C. X., Ji, Q., Meng, Q. J., Tabrum, A. R. & Luo, Z. X. Earliest evolution of multituberculate mammals revealed by a new Jurassic fossil. *Science* **341**, 779–783 (2013).
44. Xu, L. et al. Largest known Mesozoic multituberculate from Eurasia and implications for multituberculate evolution and biology. *Sci. Rep.* **5**, 14950 (2015).

Acknowledgements We thank S.-H. Xie for specimen preparation; Y.-M. Hou and P.-F. Yin for help with computed laminography scans and virtual reconstructions; X. Jin and X.-C. Guo for help with photographing and drawing; and T. Martin and J. A. Schultz for access to Guimarota specimens in the University of Bonn. We benefited from discussions with D. W. Krause, Z. X. Luo, T. Martin, J. A. Schultz, N. Kusuhashi and J. K. O'Connor. Financial support was from the Strategic Priority Research Program of the Chinese Academy of Sciences (grants XDB18000000 and XDB26000000), the National Natural Science Foundation of China (grants 41802005 and 41688103), and the State Key Laboratory of Palaeobiology and Stratigraphy (Nanjing Institute of Geology and Palaeontology, CAS; grant 183121).

Author contributions Y.W. and H.W. designed the study. H.W. organized computed tomography scans and virtual reconstructions, performed phylogenetic analyses, and prepared the main text, figures and Supplementary Information. All authors contributed to revising the manuscript and figures. Y.W. supervised all research activities.

Competing interests The authors declare no competing interests.

Additional information

Supplementary information is available for this paper at https://doi.org/10.1038/s41586-019-1792-0.

Correspondence and requests for materials should be addressed to Y.W.

Peer review information *Nature* thanks Simone Hoffmann and the other, anonymous, reviewer(s) for their contribution to the peer review of this work.

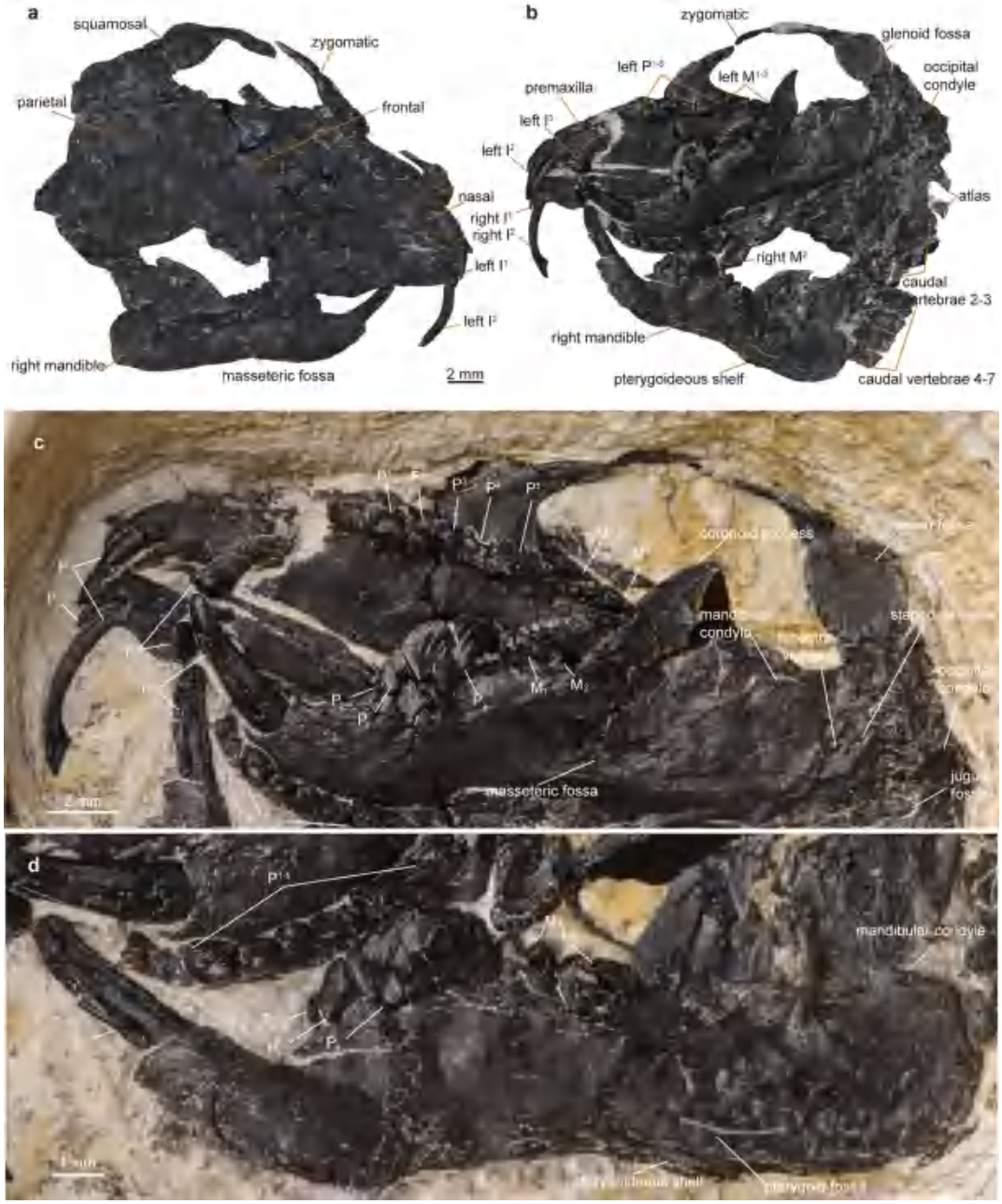

Extended Data Fig. 1 | Cranio-mandibular morphology of *J. kielanae* (holotype IVPP V20778). a, Skull in dorsal view and right mandible in lateral view. **b**, Skull in ventral view, left mandible in lateral view, and right mandible in medial view. **c**, Close-up view of cranio-mandibular features. **d**, Close-up medial view of the right dentary. The flat glenoid fossa accommodates the mandibular condyle, which is positioned below the occlusal level of the lower molars and faces posteriorly in IVPP V20778. Together with the distinct masseteric fossa—which presumably provides attachment for a well developed masseteric muscle, inserting anteriorly below P_4—the glenoid fossa produces a palinal (posterior) power stroke with distinct posterior chewing.

Extended Data Fig. 2 | Dentition of *J. kielanae* (IVPP V20778). a–**c**, Left upper cheek teeth (P^1 to M^2) in lingual (**a**), occlusal (**b**) and buccal (**c**) views. **d**, **e**, Right I^1 in medial view (**d**) and lateral view (**e**). **f**, **g**, Right I^2 in medial (**f**) and lateral (**g**) views. **h**–**j**, Right I^3 in lingual (**h**), buccal (**i**) and posterior (**j**) views. **k**, Right upper premolars (P^1 to P^5) in occlusal view. **l**, Right upper incisors (I^1 to I^3) in medial view. **m**, Right lower molars (M_1 and M_2) in occlusal view. **n**, **p**, Right lower teeth (I_1, P_2 to M_2) in lingual (**n**) and buccal (**p**) views. A, anterior; B, buccal; L, lingual; O, occlusal; P, posterior. Scale bars, 0.2 mm.

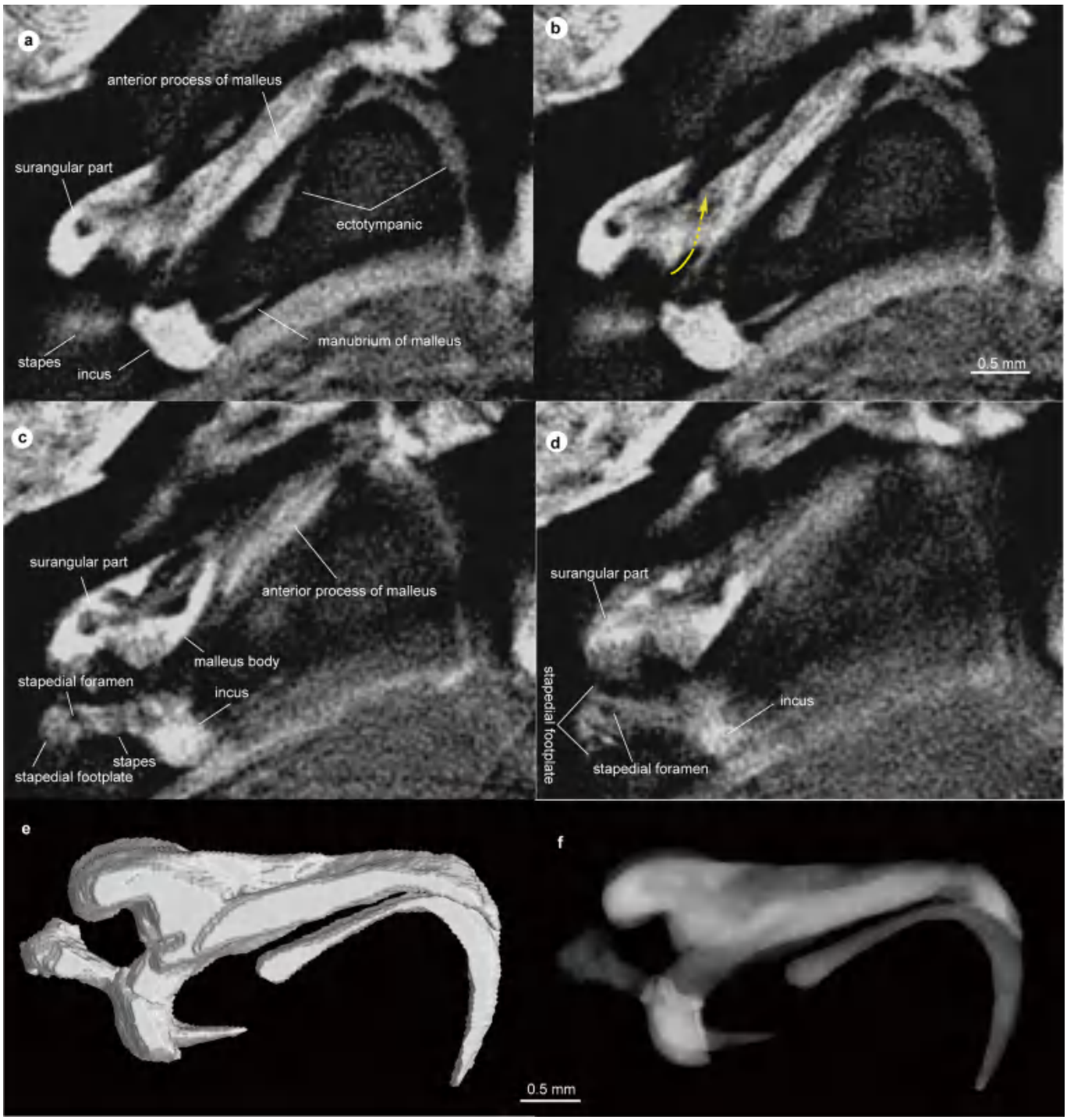

Extended Data Fig. 3 | Computed laminography images and reconstructions of left middle-ear bones. a–**d**, Computed laminography images on different levels. The path of the chorda tympani is marked with a yellow arrow in **b**. The stapedial foramen, identified by computed laminography, is shown in **c**, **d**. **e**, Three-dimensional reconstruction of left middle-ear bones in dorsal view. **f**, X-ray rendering of left middle ear, showing the differing thicknesses of different parts of the bones.

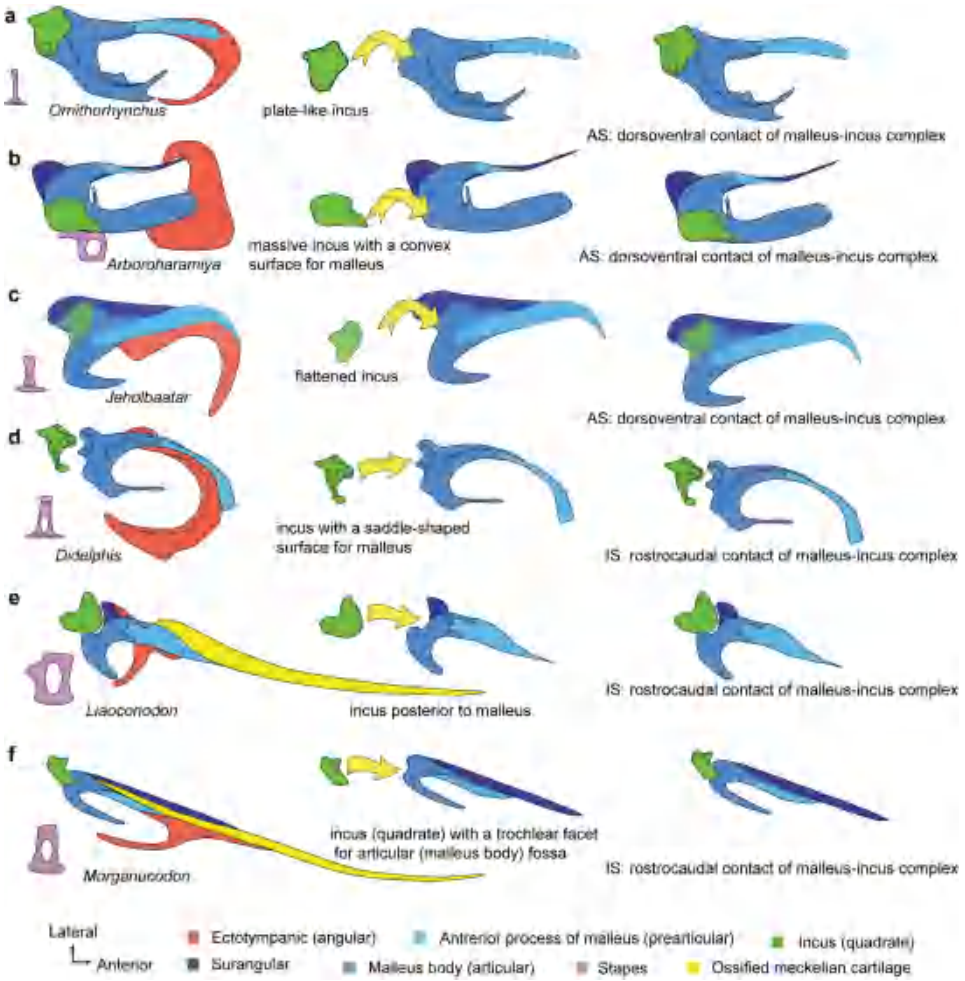

Extended Data Fig. 4 | Articular configurations of the malleus–incus complex. a, Left auditory bones of *Ornithorhynchus* in dorsal view (modified from ref. [16]). **b**, Interpretive reconstruction of left auditory bones of *Arboroharamiya* in dorsal view (modified from ref. [4]). **c**, Interpretive reconstruction of left auditory bones of *Jeholbaatar* in dorsal view. The yellow arrows in **a**–**c** show that the incus lies dorsal to the malleus in *Ornithorhynchus*, *Arboroharamiya* and *Jeholbaatar*, demonstrating the 'abutting system' (AS) arrangement of the malleus–incus complex. **d**, Left auditory bones of *Didelphis* in medial view (modified from ref. [28]), showing that the malleus–incus complex maintains the interlocking system (IS) arrangement (yellow arrow), with a rostrocaudal contact between these two elements. **e**, Left auditory bones of *Liaoconodon* in medial view (modified from ref. [3]). **f**, Left auditory bones of *Morganucodon* in medial view (modified from ref. [28]). Here the incus (quadrate) has a medial trochlear facet to contact the concave surface of the malleus body (articular fossa) posteriorly.

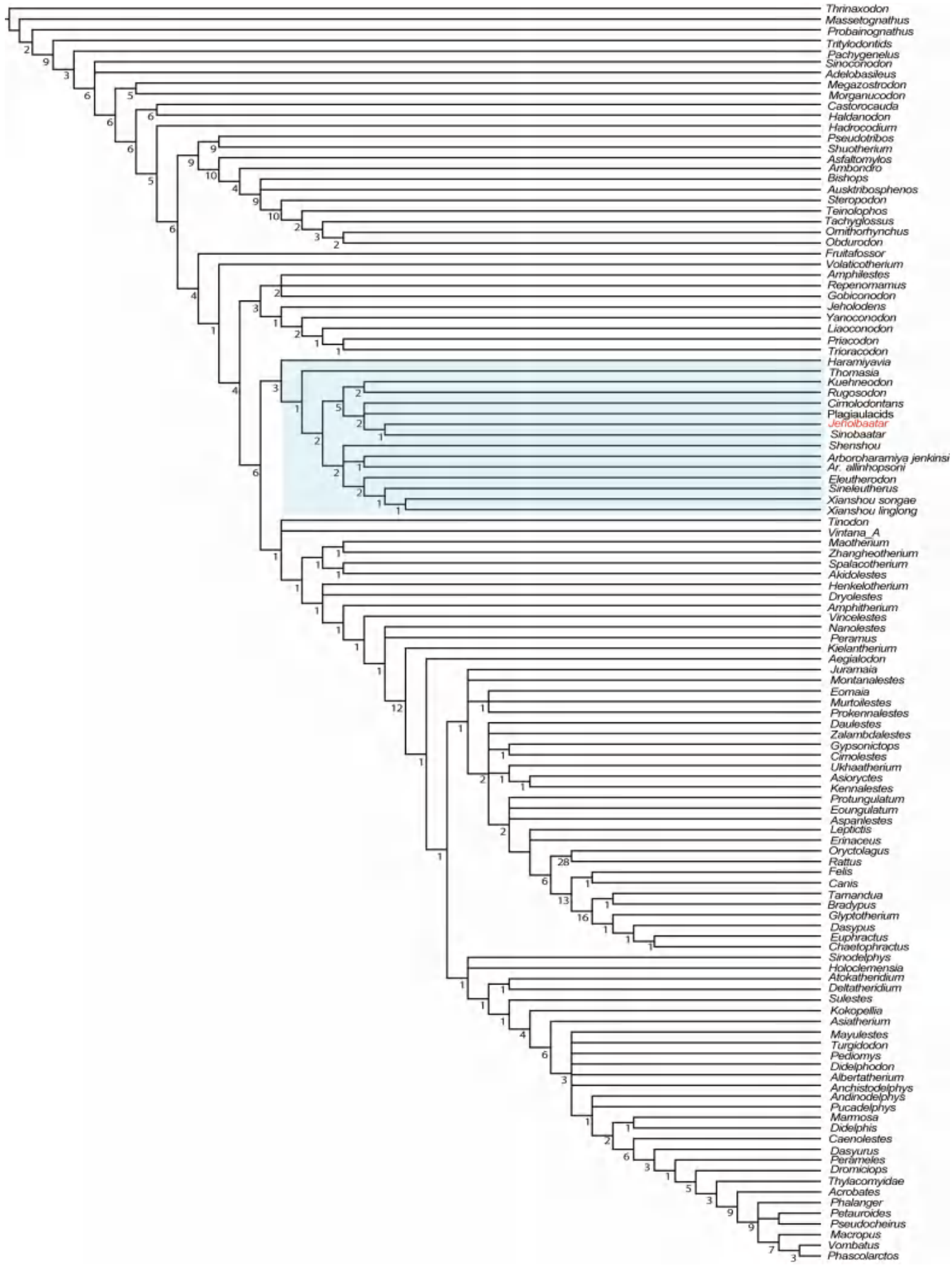

Extended Data Fig. 5 | See next page for caption.

Extended Data Fig. 5 | Strict consensus of parsimony analysis based on data matrix A. Tree length, 2,622; consistency index, 0.327; retention index, 0.795. On the basis of analysis using TNT 3.0, 14 most parsimonious trees are returned; tree length, 2,539, consistency index, 0.338; retention index, 0.804. The blue shading shows the monophyly of allotherians within crown mammals. Node supports are given as Bremer support values.

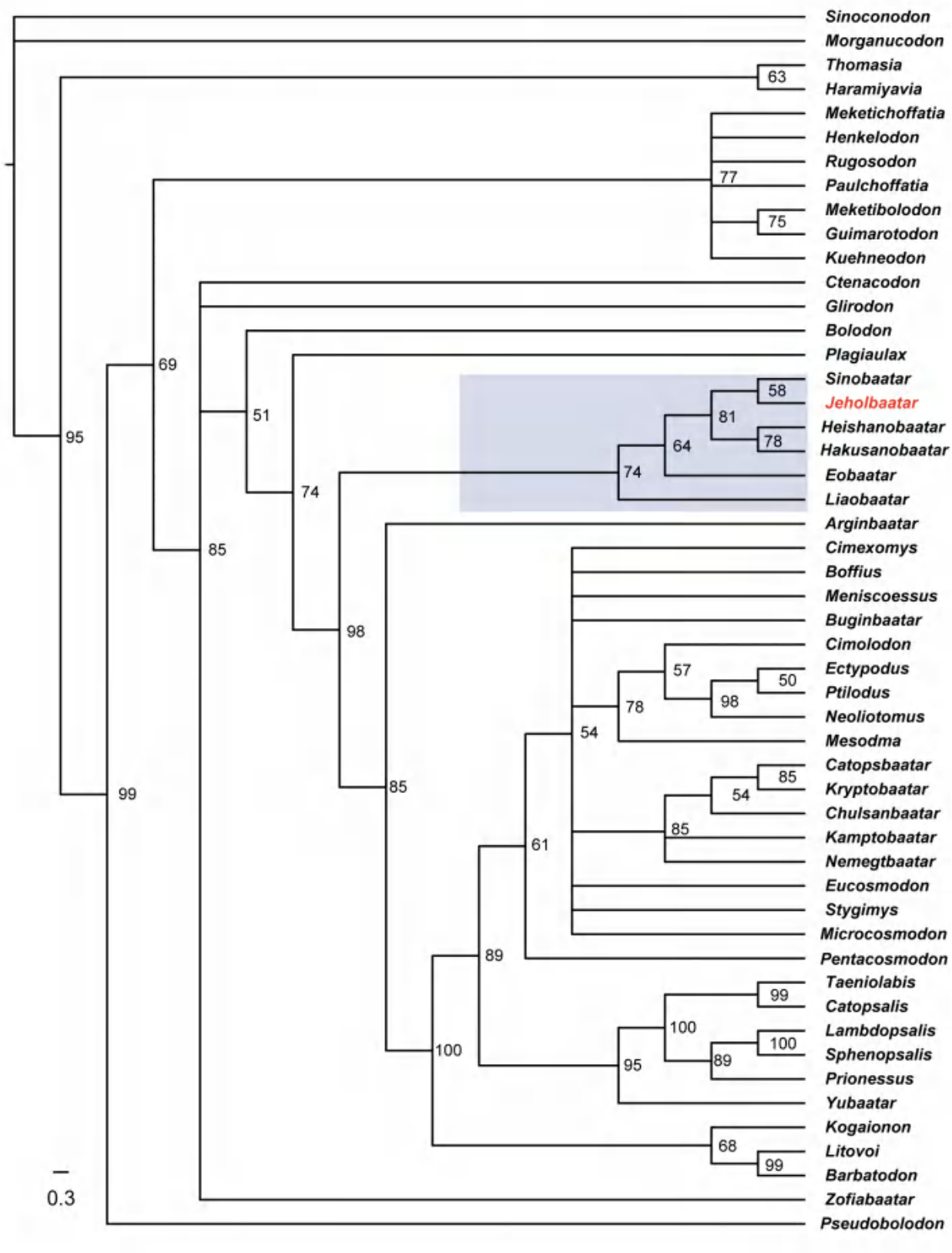

Extended Data Fig. 6 | Results of Bayesian analysis of multituberculates. This 50% majority-rule consensus was obtained from 10 million Markov Chain Monte Carlo generations with a 25% burn-in fraction. Node supports are listed as posterior probabilities (percentages). The blue rectangle shows the monophyly of eobaatarids, with *Jeholbaatar* closely related to *Sinobaatar*.

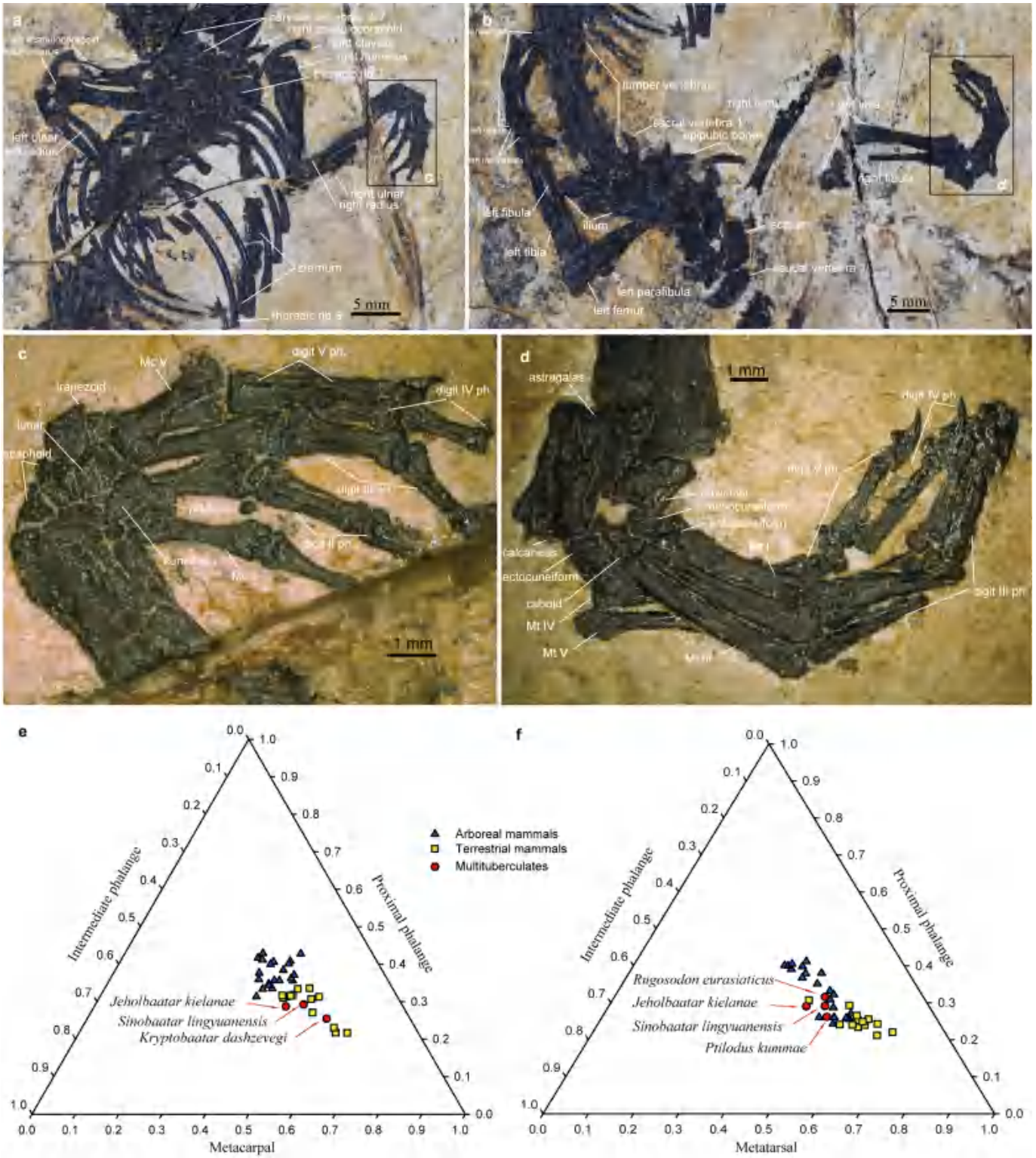

Extended Data Fig. 7 | See next page for caption.

Extended Data Fig. 7 | Manual and pedal structure, and ternary diagrams showing the proportions of phalanges from manual and pedal digit III. **a**, **b**, Shoulder (**a**) and pelvic (**b**) girdles in dorsal view. **c**, **d**, Right manus (**c**) and pes (**d**) in lateral view. **e**, **f**, Ternary plots showing ratios of metapodial (metacarpal or metatarsal), proximal and intermediate phalanges for *Jeholbaatar* digit III from the manus (**e**) and pes (**f**), and comparison with some extant terrestrial and arboreal mammals. The lengths of these three phalanges are shown as ratios of the combined length of these elements. Mc, metacarpal; Mt, metatarsal. The lengths of *Jeholbaatar* manus and pes elements (in mm, with asterisks indicating damaged elements) are: Mc I, 2.76; Mc II, *2.84; Mc III, *3.70; Mc IV, *2.81; Mc V, 2.79; digit I proximal phalanx, 1.98; digit II proximal phalanx, 2.84; digit II intermediate phalanx, *1.60; digit III proximal phalanx, 2.40; digit III intermediate phalanx, 2.26; digit IV proximal phalanx, *2.22; digit IV intermediate phalanx, 1.83; digit V proximal phalanx, 1.92; digit V intermediate phalanx, 1.54; phalange index, that is, (proximal plus intermediate)/metacarpal, digit III, 126%; Mt I, 3.92; Mt II, 4.99; Mt III, 5.42; Mt IV, *1.69; Mt V, *3.33; digit I proximal phalanx, 3.51; digit II proximal phalanx, 3.58; digit II intermediate phalanx, 2.82; digit III proximal phalanx, 3.59; digit III intermediate phalanx, 3.46; digit IV proximal phalanx, *1.73; digit IV intermediate phalanx, 3.25; digit V intermediate phalanx, 2.63; phalanx index, that is, (proximal+intermediate phalanges)/metatarsal, digit III, 130%. The manual proportion of *J. kielanae* places it closer (than the other multituberculates in the sample) to the arboreal category; the pedal proportion clusters mostly with arboreal taxa. The data for extant taxa are derived from ref. [38].

Extended Data Table 1 | Phalange indices for digit III of *Jeholbaatar* and comparison with other mammals

Taxa	Substrate	Phalange Index	
		Manual digit III	Pedal digit III
Maotherium sinensis	Terrestrial	95%	99%
Didelphis virginiana	Terrestrial	98%	88%
Eomaia scansoria	Scansorial/Terrestrial	130%	129%
Caluromys philander	Scansorial/Terrestrial	138%	156%
Arboroharamiya jenkinsi	Arboreal	246%	216%
Kryptobaatar dashzevegi	Terrestrial	81%	
Rugosodon eurasiaticus	Scansorial/Terrestrial	117%	114%
Sinobaatar lingyuanensis	Scansorial/Terrestrial	108%	109%
Ptilodus kummae	Arboreal	118%	
Eucosmodon sp.	Arboreal	119%	
Jeholbaatar kielanae	Scansorial/Terrestrial	126%	130%

nature research

Corresponding author(s): Yuanqing Wang

Last updated by author(s): Oct 14, 2019

Reporting Summary

Nature Research wishes to improve the reproducibility of the work that we publish. This form provides structure for consistency and transparency in reporting. For further information on Nature Research policies, see Authors & Referees and the Editorial Policy Checklist.

Statistics

For all statistical analyses, confirm that the following items are present in the figure legend, table legend, main text, or Methods section.

n/a	Confirmed
☒	☐ The exact sample size (*n*) for each experimental group/condition, given as a discrete number and unit of measurement
☒	☐ A statement on whether measurements were taken from distinct samples or whether the same sample was measured repeatedly
☒	☐ The statistical test(s) used AND whether they are one- or two-sided *Only common tests should be described solely by name; describe more complex techniques in the Methods section.*
☒	☐ A description of all covariates tested
☒	☐ A description of any assumptions or corrections, such as tests of normality and adjustment for multiple comparisons
☒	☐ A full description of the statistical parameters including central tendency (e.g. means) or other basic estimates (e.g. regression coefficient) AND variation (e.g. standard deviation) or associated estimates of uncertainty (e.g. confidence intervals)
☒	☐ For null hypothesis testing, the test statistic (e.g. *F*, *t*, *r*) with confidence intervals, effect sizes, degrees of freedom and *P* value noted *Give P values as exact values whenever suitable.*
☐	☒ For Bayesian analysis, information on the choice of priors and Markov chain Monte Carlo settings
☒	☐ For hierarchical and complex designs, identification of the appropriate level for tests and full reporting of outcomes
☒	☐ Estimates of effect sizes (e.g. Cohen's *d*, Pearson's *r*), indicating how they were calculated

Our web collection on statistics for biologists contains articles on many of the points above.

Software and code

Policy information about availability of computer code

Data collection	Data collection for building character matrix used in this study is based on observation of specimens.
Data analysis	Segmentation was conducted in VGStudio v.3.0. Character matrix was compiled in Mesquite v.3.03. For phylogenetic analysis, parsimony analysis was conducted in TNT v. 1.5 and Bayesian analysis was conducted in MrBayes v. 3.2. Measurements were taken in ImageJ.

For manuscripts utilizing custom algorithms or software that are central to the research but not yet described in published literature, software must be made available to editors/reviewers. We strongly encourage code deposition in a community repository (e.g. GitHub). See the Nature Research guidelines for submitting code & software for further information.

Data

Policy information about availability of data

All manuscripts must include a data availability statement. This statement should provide the following information, where applicable:

- Accession codes, unique identifiers, or web links for publicly available datasets
- A list of figures that have associated raw data
- A description of any restrictions on data availability

The specimen reported in this study is housed in an academic institute and available for scholars to examine. Data matrices were provided in Supplementary Information.

Field-specific reporting

Please select the one below that is the best fit for your research. If you are not sure, read the appropriate sections before making your selection.

☐ Life sciences ☐ Behavioural & social sciences ☒ Ecological, evolutionary & environmental sciences

For a reference copy of the document with all sections, see nature.com/documents/nr-reporting-summary-flat.pdf

Ecological, evolutionary & environmental sciences study design

All studies must disclose on these points even when the disclosure is negative.

Study description	It is a study on only one fossil specimen with phylogenetic analysis.
Research sample	It is a fossil mammal specimen from the Lower Cretaceous of Northeast China. Phylogenetic analysis is based on character matrices that cover various taxa from all mammaliaform clades with emphasis on mutituberculates.
Sampling strategy	Fossil collecting in fieldwork and specimens preparation in lab. The taxon sampling and characters selected are extensive enough to reconstruct phylogeny for both mammaliaforms and multituberculates.
Data collection	Data collection includes observation of specimens with microscope in lab and computed laminography.
Timing and spatial scale	H.W. collected data from July, 2015 to June, 2018, based on observations of specimens.
Data exclusions	No data was excluded
Reproducibility	Phylogenetic analysis is repeatable, following the method for both parsimony analysis (in TNT) and Bayesian analysis (in MrBayes) in Method section.
Randomization	N/A. It is a study on fossil material.
Blinding	N/A. Character matrices are built on the basis of independent observation for each taxon.

Did the study involve field work? ☒ Yes ☐ No

Field work, collection and transport

Field conditions	Annual average temperature is 5.4℃ ~ 8.7℃ and annual precipitation is 450-480mm.
Location	Chaoyang City, Lioaning province, China.
Access and import/export	We investigate the fossil locality, prepare the specimen, and scan the specimen at the Institute of Vertebrate Paleontology and Paleoanthropology.
Disturbance	N/A

Reporting for specific materials, systems and methods

We require information from authors about some types of materials, experimental systems and methods used in many studies. Here, indicate whether each material, system or method listed is relevant to your study. If you are not sure if a list item applies to your research, read the appropriate section before selecting a response.

Materials & experimental systems

n/a	Involved in the study
☒	☐ Antibodies
☒	☐ Eukaryotic cell lines
☐	☒ Palaeontology
☒	☐ Animals and other organisms
☒	☐ Human research participants
☒	☐ Clinical data

Methods

n/a	Involved in the study
☒	☐ ChIP-seq
☒	☐ Flow cytometry
☒	☐ MRI-based neuroimaging

Palaeontology

Specimen provenance	This specimen was discovered from the Jiufotang Formation in Changzigou site, Lingyuan county, Lioaning province, China. No permits needed for the work.
Specimen deposition	The specimen reported in this study is housed in the Institute of Vertebrate Paleontology and Paleoanthropology, Beijing, China.
Dating methods	No new dates for the specimen.

☒ Tick this box to confirm that the raw and calibrated dates are available in the paper or in Supplementary Information.